FRONTIERS OF PHYSICS

RESEARCH ARTICLE
Volume 19 / Issue 4 / 43208 / 2024

Modulation of charge in C_9N_4 monolayer for a high-capacity hydrogen storage as a switchable strategy

Lin Ju[1,†], Junxian Liu[2], Minghui Wang[1], Shenbo Yang[3], Shuli Liu[1]

1 School of Physics and Electric Engineering, Anyang Normal University, Anyang 455000, China
2 School of Mechanical, Medical and Process Engineering, Queensland University of Technology, Brisbane QLD 4001, Australia
3 Hongzhiwei Technology (Shanghai) Co. Ltd., 1599 Xinjinqiao Road, Pudong, Shanghai 201206, China
Corresponding author. E-mail: †julin@aynu.edu.cn
Received December 14, 2023; accepted January 16, 2024

ABSTRACT

Developing advanced hydrogen storage materials with high capacity and efficient reversibility is a crucial aspect for utilizing hydrogen source as a promising alternate to fossil fuels. In this paper, we have systematically investigated the hydrogen storage properties of neutral and negatively charged C_9N_4 monolayer based on density functional theory (DFT). Our foundings indicate that injecting additional electrons into the adsorbent significantly boosts the adsorption capacity of C_9N_4 monolayer to H_2 molecules. The gravimetric density of negatively charged C_9N_4 monolayer can reach up to 10.80 wt% when fully covered with hydrogen. Unlike other hydrogen storage methods, the storage and release processes happen automatically upon introducing or removing extra electrons. Moreover, these operations can be easily adjusted through activating or deactivating the charging voltage. As a result, the method is easily reversible and has tunable kinetics without requiring particular activators. Significantly, C_9N_4 is proved to be a suitable candidate for efficient electron injection/release due to its well electrical conductivity. Our work can serve as a valuable guide in the quest for a novel category of materials for hydrogen storage with high capacity.

Keywords hydrogen storage, C_9N_4 monolayer, charge modulation, density functional theory

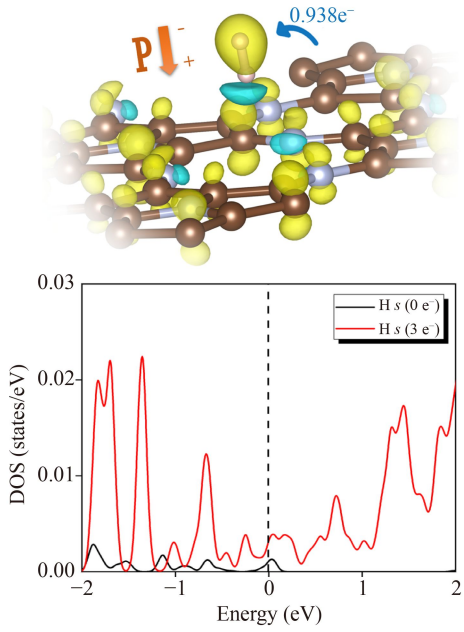

1 Introduction

Hydrogen has been regarded as a kind of promising substitute for fossil fuels in different energy applications due to the plentiful supply, high energy density, environmentally friendly combustion, as well as renewable potential [1, 2]. Nevertheless, a critical hindering its commercial application lies in the development of a storage medium that is both safe and practical [3, 4]. The ideal hydrogen storage materials for practical use must meet strictest criteria, encompassing the ability to store hydrogen reversibly, while high volumetric and gravimetric densities are achieved [5]. As reported by the 2010 U.S. Department of Energy (U.S. DOE), the goals of hydrogen storage materials should meet gravimetric and volumetric densities of at least 6 wt% and 45 $g{\cdot}L^{-1}$, respectively. To enable reversible hydrogen storage/release under near-ambient conditions, the adsorption energy for H_2 molecules needs to fall within the range from –0.20 to –0.60 eV/H_2 [6]. Light-metal and

Higher Education Press

https://doi.org/10.1007/s11467-023-1385-0

nonmetal hydrides are among the candidate materials suitable for high-capacity hydrogen storage [7]. The listed compounds, like $B_{12}H_{12}$, BH_3, and $NaAlH_4$, consist of bound hydrogen atoms, which pose challenges in catalysis for breaking the H_2 bond and ensuring efficient loading kinetics. But if the intrinsic binding energy of H_2 is too strong, the kinetics of hydrogen release is also adversely affected. Another option for candidate materials involves utilizing light-element-based materials [8], like carbon nanotubes or other nanostructures, non-carbon-based nanotubes, mesoporous silica, and covalent-organic frameworks (COFs) [9, 10]. With adsorption energies in the meV range, the absorbent material weakly bind to the H_2 molecule, leading to its desorption at extremely low temperatures. High pressures are necessary to ensure sufficient storage due to the weak adsorption energetics. Additional researches reveal that, the addition of a small amount of alkali metals (such as Na, Li, and Ca) significantly boosts the binding strength between carbon nanostructures and H_2 molecules [11–14]. In the case of transition metals (such as Sc, Ti, and V), the H_2 molecule tends to stay at the special metal site due to an interaction combining physisorption and chemisorption [15–17]. However, how to prevent the aggregation of adsorbent metal atoms and the resulting degradation of H_2 storage performance remains a challenge [18–20]. Theoretical findings, in Yoon *et al.*'s study [21], indicate that charging fullerenes increases the adsorption of H_2 molecules, potentially achieving high-capacity hydrogen storage. However, experimental control over the charging of fullerenes is challenging. Theoretical research, conducted by Niu *et al.* [22], demonstrates the potential for molecular binding of H_2 when it is near a positively charged transition-metal ion. Zhou *et al.* [23] have suggested an alternative method for tackling the aforementioned issues concerning hydrogen storage, ensuring efficient reversibility and speedy kinetics. Take boron nitride (BN) as an example, applying an electric field to produce a polarized substrate can significantly improve its hydrogen storage performance. The storage capacity of the BN sheets increases by 7.5 wt% and the release of stored H_2 molecules becomes easy once the electric field is removed, allowing for fast and reversible storage. Nevertheless, the necessary electric field of 23 000 $MV \cdot m^{-1}$ is excessively huge and impractical for daily use. To decrease the necessary electric field, researchers propose using a substrate with higher polarizability (such as AlN and $H_8Si_8O_{12}$) sheets. While this achieves the required energy for H_2 adsorption with a reduced electric field, for $H_8Si_8O_{12}$ and AlN, the gravimetric densities of stored hydrogen drop significantly to 2.6 and 4.5 wt% respectively. These values fall below the hydrogen storage target set by the U.S. DOE in 2010.

Graphitic carbon nitrides, emerging two-dimensional conjugated polymers, have recently gained significant attentions due to their unique anisotropic geometric morphologies and aromatic p-conjugated frameworks [4, 24]. The chemical formula of these 2D allotropes is C_xN_y, in which x and y are on behalf of the amount of C and N atoms in the unit cell, respectively. They exhibit robust and stable characteristics due to the strong covalent bonds formed between C–C and C–N bonds. The electronic, optical, electrochemical, mechanical, and thermal conduction properties of these carbon nitride allotropes depend on the composition of C and N atoms in different atomic lattices [25]. Their suitable bandgap and surface-engineered qualities make them ideal candidates for a variety of energy and environmental applications [26], such as photocatalytic water splitting [27–29], hydrogen production [30], CO_2 conversion [31], organosynthesis [32], and others [33]. Moreover, the maximum hydrogen storage mass density for Li, Na, and K decorated C_9N_4 monolayers have been reported to reach 7.04, 8.70, and 8.10 wt%, respectively [34, 35]. Those findings suggest that C_9N_4 monolayer has the potential to be used as a hydrogen storage material. However, it remains a major challenge to address the decrease in hydrogen mass density due to the introduction of metal atoms to form metal nanoclusters, which is currently the major obstacle to overcome in utilizing C_9N_4 for hydrogen storage. Recently, charge modulation has been found to be a reliable method for the enhancement of H_2 storage performance of g-C_4N_3 monolayer [36]. Inspired by the exciting result, in this work, we systematically study the hydrogen storage performance of C_9N_4 monolayer and the charge modulation induced enhancement on it through first-principle calculations.

Our work suggests that efficient hydrogen storage could be achieved by adjusting the charge state of g-C_9N_4 nanosheet. The injection of four extra electrons into the adsorbent can significantly decrease the adsorption energy of H_2 molecules on g-C_9N_4 from 0.23 eV to approximately −1.27 eV. When completely covered by hydrogen, negatively charged g-C_9N_4 can achieve gravimetric density of up to 10.8 wt%. The stored H_2 molecules can be readily desorbed from the adsorbent by removing the additional electrons. Notably, unlike other methods of hydrogen storage, the storage and release of H_2 happen naturally, and the control and reversible nature of these processes can be easily achieved by turning the charging voltage on or off. Moreover, given the excellent electrical conductivity and high electron mobility, the experimental modification is flexible to adjust the charge states of g-C_9N_4. Our predictions could greatly aid in the search for a new type of hydrogen storage materials that possess optimal reversibility and thermodynamics, providing a high storage capacity.

2 Computational methods

The DS-PAW package is used to implement our DFT calculations [37]. We adopt the Perdew–Burke–Ernzerhof (PBE) [38] and Heyd–Scuseria–Ernzerhof (HSE06) [39]

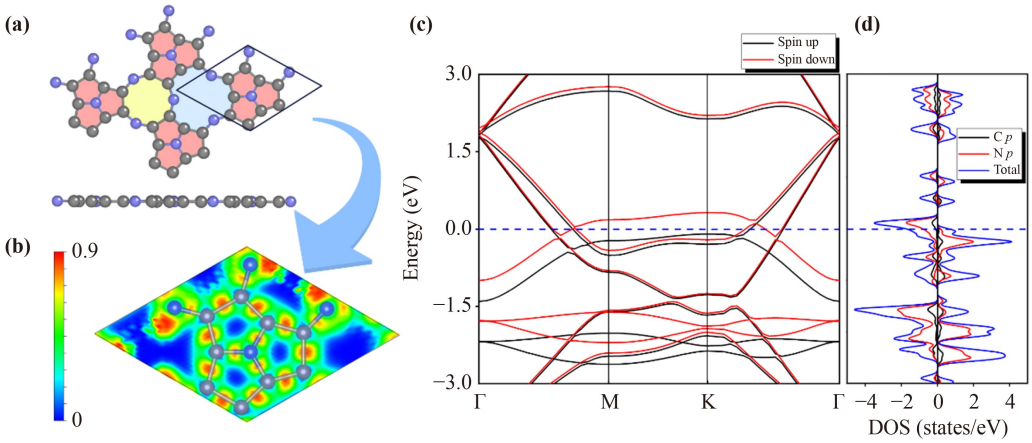

Fig. 1 **(a)** Top and side views of a reconstructed C_9N_4 monolayer. The N and C atoms are symbolized by the blue and grey balls correspondingly. **(b)** Electron localization functions. **(c)** The electronic band structure and **(d)** the projected density of states, relative to the Fermi level, which is represented by the blue dashed line.

functional in conjunction with a generalized gradient approximation (GGA). Our computations utilize a DFT+D3 approach in Grimme's scheme to describe the van der Waals (vdW) correction [40, 41]. To examine the interaction between H_2 molecules and C_9N_4 nanosheets, we put a H_2 molecule on a 1×1 C_9N_4 cell, employing periodic boundary conditions in the x–y plane. To prevent interactions between periodic images, the vacuum space along the z direction is increased to more than 20 Å. In geometric optimizations, all atomic coordinates are entirely relaxed, guaranteeing that the residual atomic forces are less than 0.05 eV/Å, and the total energy is converged to 10^{-4} eV. A $5 \times 5 \times 2$ Monkorst-Pack k-point mesh is used to simulate the Brillouin zone interaction. The average adsorption energy of the adsorption system composed by n H_2 molecules adsorbing on the C_9N_4 monolayer is defined as

$$\bar{E}_{\text{ads}} = (E_{\text{total}} - n_{H_2} E_{H_2} - E_{C_9C_4})/n_{H_2}, \quad (1)$$

where $E_{C_9C_4}$, E_{H_2}, E_{total}, and n_{H_2} stand for the total energy of isolated C_9N_4 monolayer, an individual H_2 molecule, the adsorption system, and the amount of the adsorbed H_2 molecules. When $n_{H_2} = 1$, the $\bar{E}_{\text{ads}}$ stands for the adsorption energy of one H_2 molecule adsorbing on the C_9N_4 monolayer. Based on this definition, the greater the negative adsorption energy, the stronger the binding of the H_2 molecule to the adsorbent. With the Bader method, the determination of electron distribution and transfer mechanism is accomplished.

Plane integration charge density difference (CDD) is performed using the following formula [42]:

$$\Delta\rho = \rho_{\text{total}} - \rho_{C_9N_4} - \rho_{H_2}, \quad (2)$$

where ρ_{H_2} and $\rho_{C_9N_4}$ are defined as the charge densities of the adsorbed H_2 molecule and C_9N_4 monolayer, respectively. ρ_{total} represents the charge density of the adsorption configuration.

To measure the stability of the C_9N_4 monolayer, the binding energy E_b is calculated using the following equation [43]:

$$E_b = (E_{C_9N_4} - n_C E_C - n_N E_N)/(n_C + n_N), \quad (3)$$

where $E_{C_9N_4}$, n_C, n_N E_C and E_N are defined as the total energy of the C_9N_4 monolayer, the numbers of C and N atoms in the unit cell, the energies of the isolated C and N elements, respectively.

3 Result and discussion

3.1 Geometric and electronic structures of C_9N_4 monolayer

We first investigate the geometric and electronic structures of C_9N_4 monolayer. Figure 1(a) illustrates the hexagonal atomic lattices of the energy minimized C_9N_4 monolayer. These hexagonal atomic lattices consisting of porous structures are formed by three pentagon cores [pink areas in Fig. 1(a)] connected by the N atoms. The porous structures exhibit repetitive 12 and 9 membered rings [yellow and blue areas in Fig. 1(a), respectively] composed of covalent networks of C and N atoms. The hexagonal lattice constant of C_9N_4 monolayers is measured to be 6.95 Å, which is considerably very close to the previously observed lattice value of 6.88 Å [43]. In the single layer C_9N_4, the C–C bond length in the 9-membered rings is 1.56 Å, while the one in the 12-membered rings is 1.46 Å. Clearly, the C–N bonds, serving as connectors of pentagon cores, exhibit the shortest bond lengths, indicative of their high rigidity. Conversely, the C–C bonds in the 9 membered rings are the longest bonds in the nanosheet. As displayed in Fig. 1(b), the electron localization function (ELF) demonstrates that, the electron localization is around the center of all the C–C and C–N bonds, confirming the

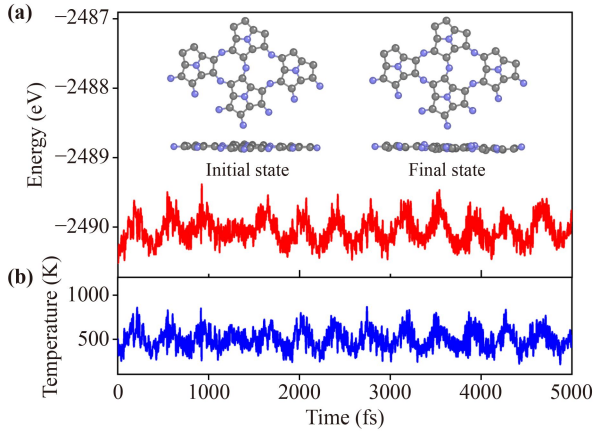

Fig. 2 **(a)** AIMD simulations on total energy for C_9N_4 monolayer for 5 ps with a time step of 1 fs at 500 K. **(b)** The corresponding temperature for each step.

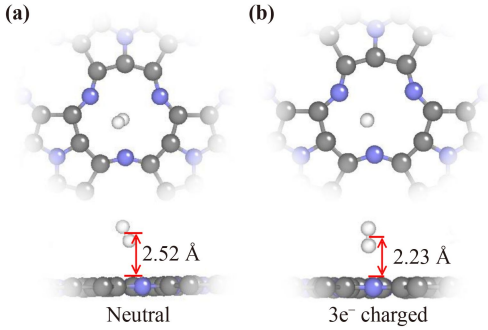

Fig. 3 Top and side views of the lowest-energy configurations of **(a)** neutral and **(b)** $3e^-$ charged C_9N_4 monolayers with a H_2 molecule absorbed on them, respectively. The blue, grey and white balls represent N, C, and H atoms, respectively. The adsorption distance, which is apart from the barycenter of the adsorbed H_2 molecule to the surface of the C_9N_4 monolayer, is marked out in the figure.

prevalence of covalent bonding in these innovative nanomaterials. Strong electron localization is also around the N atoms acting as connectors of pentagon cores. The binding energy for C_9N_4 monolayer is calculated to be –8.50 eV/atom, almost the same as the previous result (– 8.46 eV/atom) reported by Mortazavi's group [43], who has confirmed the dynamical and structural stability of C_9N_4 monolayer based on the phonon dispersion calculation results. Besides, the stability and reducibility of a novel material are typically determined by the thermal stability, a crucial factor in their overall performance. *Ab* initio molecular dynamics (AIMD) simulations are conducted for 5 ps at the temperature of 500 K to evaluate the thermal stability of the C_9N_4 monolayer. The slight fluctuation in total energy and the minor geometric reconstructions reveal that, C_9N_4 nanosheet can remains completely intact at temperature up to 500 K (see Fig. 2). Both the dynamic and thermal stabilities of C_9N_4 nanosheet offer promising insights into its potential for experimental synthesis and practical applications at room temperature.

Next, we explore the electronic characteristics of the C_9N_4 nanosheet by calculating the electronic band structure along the high symmetry Γ– M– K– Γ path and density of states (DOS) using the PBE/GGA method. The electronic band structure of the C_9N_4 monolayer, depicted in Fig. 1(c), reveals an overlap of the conduction and valence bands at the Fermi level, indicating metallic electronic features, which differs from most carbon nitride 2D systems with semiconductor properties. As displayed in Fig. 1(d), the corresponding DOS shows that, the Fermi level is crossed by both N 2*p* and C 2*p* orbitals, which is the origin of the metallic character. Considering that the PBE function usually underestimates the band gap, we use the HSE06 hybrid function to obtain a more accurate electronic band structure. As shown in Fig. S1 of the Electronic Supplementary Materials (ESM), the HSE06 result favors the conclusion that the C_9N_4 monolayer is metallic as well. The metallicity means that C_9N_4 possesses favorable electrical conductivity, making it conducive for efficient electron injection and release. This property is particularly advantageous for charge-controlled switchable hydrogen storage applications.

3.2 Single H_2 molecule adsorption on neutral and negatively charged C_9N_4 nanosheets

In our investigation of the C_9N_4 monolayer's hydrogen storage capabilities in the following, we initially explore the H_2 adsorption on neutral C_9N_4 nanosheets. As shown in Fig. S2 of the ESM, on the surface of C_9N_4 monolayer, there are two kinds of N and C atoms, respectively. We separately mark them as N1 (three-coordinated N atom), N2 (two-coordinated N atom), C1 (C atom attached to N1 atom), and C2 (C atom attached to N2 atom). Besides, as mentioned above, there are three regions, i.e., five-membered, nine-membered, and twelve-membered rings. Therefore, we considered 7 kinds of sites for H_2 molecule adsorption, which are the top of (i) five-membered ring, marked with **F**, (ii) nine-membered ring, marked with **Nr**, (iii) twelve-membered ring, marked with **T**, (iv) N1 atom, marked with **N1**, (v) N2 atom, marked with **N2**, (vi) C1 atom, marked with **C1**, (vii) C2 atom, marked with **C2**.

As listed in Table S1 of the ESM, among the considered cases, the configuration where the H_2 molecule is absorbed at the **T** site [see Fig. 3(a)] exhibits the lowest total energy, indicating the most favorable adsorption site. In this configuration, the adsorbed H_2 molecule is aligned perpendicular to the surface of C_9N_4 monolayer, and situated 2.52 Å vertically away from the C_9N_4 monolayer, while the bond length between the two hydrogen atoms is 0.76 Å. In the neutral state, the H_2 molecule demonstrates a weak interaction with C_9N_4,

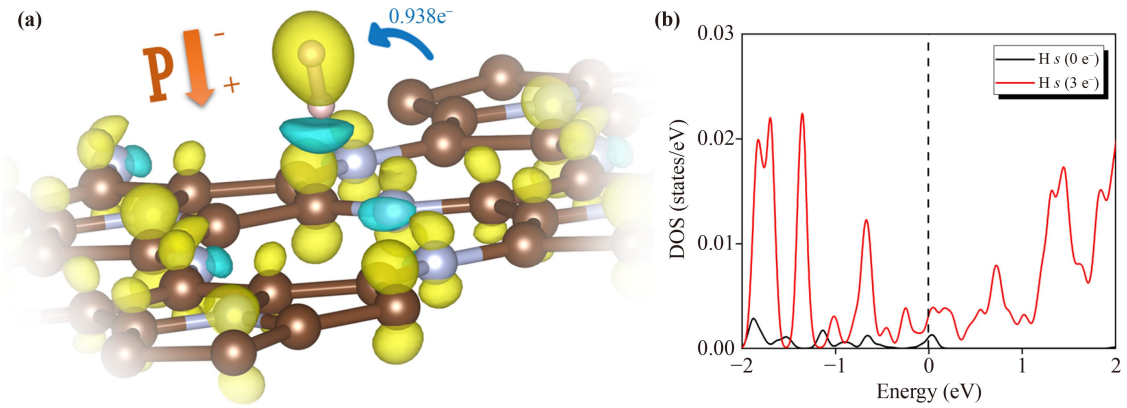

Fig. 4 **(a)** The charge density difference for the adsorption system, constructed by a H_2 molecule adsorbing on $3e^-$ negatively charged C_9N_4. Yellow and cyan regions refer to the electron-rich and -deficient areas, respectively. The isosurface value is 7×10^{-4} e/au. **(b)** The H *s*-orbital from the adsorbed H_2, before and after the introduction of three electrons, with the dashed line being the Fermi energy level.

resulting in an adsorption energy of 0.24 eV/H_2. The positive value of the adsorption energy indicates an endothermic adsorption process. By comparison, the inverse process, the desorption process, is exothermic and can occur spontaneously.

Then, we inject three additional electrons into the C_9N_4 monolayer, and obtain the most stable configuration for the H_2 adsorption [Fig. 3(b)]. The H_2 molecule, that is perpendicular to C_9N_4 monolayer, still is situated in close proximity on the **T** site. However, compared to the case of the H_2 molecule adsorption on neutral C_9N_4 monolayer, the vertical adsorption distance decreases from 2.52 to 2.23 Å, while the H–H bond length increases from 0.75 to 0.76 Å. Moreover, the adsorption energy is significantly decreased to –1.08 eV/H_2, indicating a spontaneous adsorption process for the H_2 molecule on the $3e^-$ negatively charged C_9N_4 monolayer.

The significant enhancement in the adsorption capacity of the negatively charged C_9N_4 monolayer probably comes from the enhanced electrostatic interactions between the adsorbate and adsorbent, which depends on the charge transfer at the interface. According to Bader analysis, we find that there is almost no charge transfer (merely $0.003e$) between the H_2 and neutral C_9N_4 monolayer. As the increasing number of injected electrons in C_9N_4 monolayer, there is a significant increase in the electron transfer from negatively charged C_9N_4 monolayer to the absorbed H_2 molecule. For instance, the adsorbed H_2 molecule obtains up to $0.94e$ from the $3e^-$ negatively charged C_9N_4 monolayer. It is noteworthy that the H atom, closer to the adsorbent, carries a positive charge ($+0.14e$), while the other H atom carries a negative charge ($-1.08e$), implying that the electrons of the H_2 molecule are polarized.

To comprehend the interfacial charge transfer, we visualize it by computing the CDD. As plotted in Fig. 4(a), an electron-rich area (yellow region) is distributed on the upper H atom, while an electron-depleted area (cyan region) is observed on the lower H atom, which verifies the polarization of the adsorbed H_2 molecule. The possible explanation for the polarization could be expressed as follows. A larger number of electrons are aggregated on the C atoms (yellow region) and delocalized over the N atoms (cyan region). The presence of charge reconstruction at the surface of $3e^-$ negatively charged C_9N_4 monolayer creates a strong electric field [44], which, in turn, polarizes the adsorbed H_2 molecule, significantly increasing the adsorption capacity of the negatively charged C_9N_4 for H_2 molecules. In addition, we also calculate the density of states of the adsorbed hydrogen molecule with (red line) and without (black line) the introduction of the three extra electrons. Clearly, after the three extra electrons are introduced into the adsorbent, the peaks of the *s*-orbitals of the H_2 molecule near the Fermi energy level are obviously increased, indicating that the activity of the hydrogen molecule has been greatly enhanced, aligning with the conclusions drawn above.

To comprehensively explore the relationship between the details of H_2 adsorption and the number of injected electrons in the adsorbent, we calculate the changes in H–H bond length, vertical adsorption distance, adsorption energy, and H_2 dipole moment in the adsorption system for different charged states of the adsorbent. As displayed in Fig. 5(a), the H–H bond length exhibits a slight increase (less than 1.99%) with the rising number of injected electrons, which indicates that the shape of the adsorbed hydrogen molecule remains intact and is not obviously affected by the external charges. However, as shown in Fig. 5(b), along with the increasing injected electrons, there is a pronounced decrease (up to 15.48%) in the vertical adsorption distance between the H_2 molecule and the adsorbent, from 2.52 Å (neutral state) to 2.13 e·Å ($5e^-$ charged state). The decreased adsorption

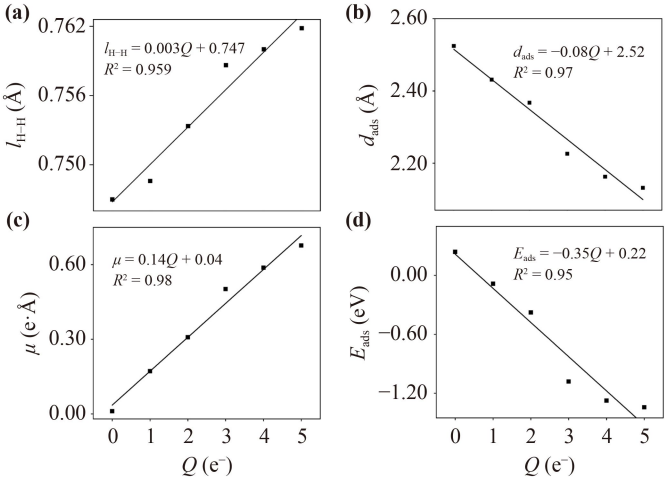

Fig. 5 **(a)** The H–H bond length, **(b)** vertical distance from H_2 to C_9N_4, **(c)** induced dipole moment of H_2 molecule and **(d)** adsorption energy as well as their corresponding fittings, with respect to the amount of charge introduced (Q). Q could represent the valence of C_9N_4 monolayer. R^2 is the correlation coefficient.

distance predicts an enhanced interaction between the adsorbed H_2 molecule and adsorbent, originating from the polarization of adsorbed H_2 molecule, as discussed before. The increase in electron density, resulting from the increasing injected electrons, amplifies the electric field at the surface of the negatively charged C_9N_4 monolayer, therefore, leading to a shift in the electronic polarization of the adsorbed H_2 molecule. This shift is evident in the raised dipole moment, as illustrated in Fig. 5(c), increasing from 0.01 e·Å (neutral state) to 0.68 e·Å ($5e^-$ charged state). Not surprisingly, the adsorption energies of a H_2 molecule on C_9N_4 monolayer become more negative, as the number of the injected electrons increases. For the traditional hydrogen storage materials, excessively negative adsorption energies usually ask for an extremely high temperature to release the adsorbed H_2 molecule, which may lead to serious energy consumption and the decomposition of the hydrogen storage materials. So that, the U.S. DOE standard requires the ideal adsorption energies larger than –0.60 eV/H_2. However, for the negatively charged C_9N_4 monolayer, the release of hydrogen only requires the removal of the extra charge, making it nearly temperature-independent. From this standpoint, the more negative the adsorption energy, the better the hydrogen storage performance of C_9N_4 monolayer. As shown in Fig. 5(d), the adsorption energy falls below –0.38 eV/H_2 when the number of injected electrons exceeds two, satisfying the upper limit (≤ –0.20 eV/H_2) requirement from U.S. DOE standard for the adsorption. Therefore, the negatively charged C_9N_4 monolayer proves to be an exceptional medium for hydrogen storage.

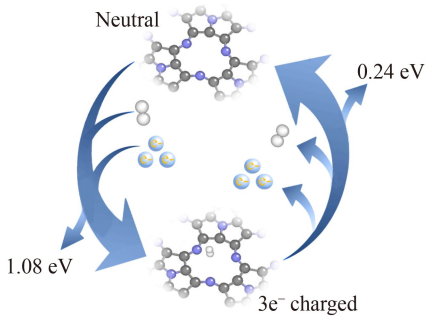

Fig. 6 Reversible energy cycle diagram of C_9N_4 monolayer adsorbing and releasing an H_2 molecule through introducing and removing electrons.

3.3 Potential kinetic pathways for hydrogen storage/release on C_9N_4 monolayer

To elucidate the potential kinetic pathways for hydrogen storage/release on the C_9N_4 monolayer, we examine the energy transformation during these two processes. Herein, as illustrate in Fig. 6, we take the case of addition/removal of the three extra electrons into the C_9N_4 monolayer as an example. During the H_2 adsorption process, introducing three additional electrons into C_9N_4 causes a significant increase in the interactions between the H_2 molecule and the $3e^-$ negatively charged C_9N_4, leading to the spontaneous binding of the H_2 molecule with an adsorption energy of –1.08 eV/H_2. The process exhibits an exothermic nature with a heat release of 1.08 eV/H_2. In contrast, when three electrons are extracted from the $3e^-$ negatively charged C_9N_4 monolayer, the H_2 molecule naturally returns to a weakly bonded state and detaches from C_9N_4 surface. This transition releases energy amounting to 0.24 eV/H_2. In order to remove the electrons smoothly, it is likewise necessary for C_9N_4 to maintain its metallicity after adsorbing H_2 molecules. To validate this issue, we calculate the DOS of C_9N_4 monolayer in this case. As shown in Fig. S3 of the ESM, some electronic states pass the Fermi energy level, indicating that the C_9N_4 monolayer with the introduction of a H_2 molecule still maintains its metallicity. Consequently, the process of adsorbing and releasing hydrogen on C_9N_4 monolayer is reversible, and it exhibits rapid kinetics. Additionally, the control of these two processes can be easily achieved by introducing or removing extra electrons.

3.4 The gravimetric density of stored hydrogen on negatively charged C_9N_4 monolayers

According to the results of adsorption energy shown in Fig. 4(d), the $3e^-$–$5e^-$ negatively charged C_9N_4 monolayers have a relatively more negative value (less than –1.00 eV), so we choose these three cases to study the gravimetric density of stored hydrogen on negatively charged C_9N_4 monolayers. As shown in Figs. S4, S5, and

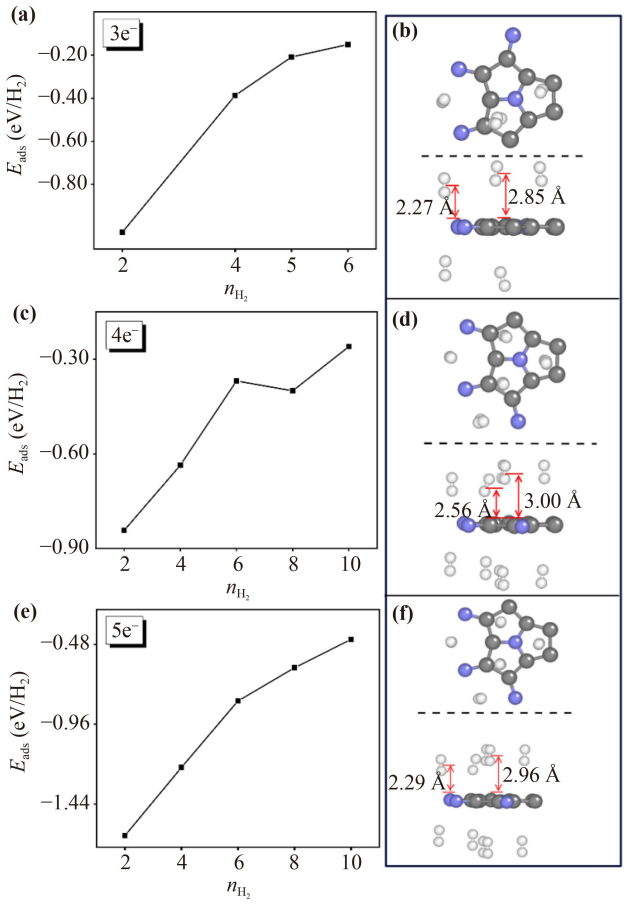

Fig. 7 Average adsorption energy of H_2 on the **(a)** $3e^-$, **(c)** $4e^-$, and **(e)** $5e^-$ negatively charged C_9N_4 monolayer with different coverage. Top and side views of the lowest-energy configuration of **(b)** $3e^-$, **(d)** $4e^-$, and **(f)** $5e^-$ negatively charged C_9N_4 at full hydrogen coverage.

S6 of the ESM, on the $3e^-$–$5e^-$ negatively charged C_9N_4 monolayers, we separately add one hydrogen molecule to each of the top and bottom symmetric positions at a time. That is to say, we add two hydrogen molecules every time.

For the case of $3e^-$ negatively charged C_9N_4 monolayers, when the number of the introduced hydrogen molecules equals to six ($n_{H_2} = 6$), the average adsorption energy is [–0.15 eV/H_2, seeing Fig. 7(a)], which is already over the highest average adsorption energy of U.S. DOE standard (−0.20 eV/H_2). Then, we test the case of $n_{H_2} = 5$, and the optimized adsorption structure is shown in Fig. 7(b). The average adsorption energy is –0.21 eV/H_2, falling within the average adsorption energy of U.S. DOE standard. But in this case, the hydrogen storage mass density is only 5.70 wt%, which does not satisfy the U.S. DOE standard for hydrogen storage mass density (6.5 wt%).

As illustrated in Fig. 7(c) and Fig. S3 of the ESM, the $4e^-$ negatively charged C_9N_4 has the capacity to capture a maximum of 10 H_2 molecules, with a decrease in average adsorption energy from − 1.27 eV/H_2 (n_{H_2} = 1) to –0.26 eV/H_2 ($n_{H_2} = 10$). As shown in Fig. S7 of the ESM, due to the steric hindrance effect between the H_2 molecules during adsorption, the introduction of more hydrogen molecules ($n_{H_2} = 12$) causes a release of hydrogen molecules, whose adsorption distance is over 4 Å, undoubtedly beyond the van der Waals force region. As a result, we decide that $n_{H_2} = 10$ is a probable threshold for complete hydrogen coverage, and the optimized configuration is shown in Fig. 7(d). Significantly, the gravimetric density of stored hydrogen is 10.8 wt%, greatly surpassing the U.S. DOE standard for hydrogen storage mass density. It is also larger than many traditional hydrogen storage two-dimensional materials, such as Ti decorated graphene (7.80 wt%.) [45], Li decorated penta-octa-graphenes (9.90 wt%) [46], Ti decorated penta-octa-graphenes (6.50 wt%) [46], Li decorated boron phosphide (4.92 wt%) [47], Na decorated boron phosphide (4.56 wt%) [47], Na decorated boron monolayer (6.80 wt%), and Ca decorated boron monolayer (7.60 wt%) [48]. Moreover, with regard to raising the hydrogen storage mass density of C_9N_4 monolayer, introducing extra electrons is more efficient than introducing extra single metal atoms. For Li, Na, and K decorated C_9N_4 monolayers, the maximum hydrogen storage mass density (7.04, 8.70, and 8.10 wt%, repectively) [34, 35] are all below the one of $4e^-$ negatively charged C_9N_4 monolayer (10.80 wt%).

At last, we conduct the calculations on the hydrogen storage mass density of $5e^-$ negatively charged C_9N_4 monolayer. Our calculations reveal that, the hydrogen storage mass density of the $5e^-$ negatively charged C_9N_4 monolayer is the same as that in the $4e^-$ negatively charged C_9N_4 monolayer. Comparatively speaking, the average adsorption energy [–0.45 eV/H_2, see Fig. 7(e)] under the case of $n_{H_2} = 10$ for the $5e^-$ negatively charged C_9N_4 monolayer is lower than the one (–0.26 eV/H_2) for the $4e^-$ negatively charged C_9N_4 monolayer. Substantially enhanced repulsive force between the adsorbed molecules in the excessive density led to the escape of adsorbed H_2 molecules, as we continued to introduce H_2 molecules on the $n_{H_2} = 10$ adsorption system (seeing Fig. S6 of the ESM). So, $n_{H_2} = 10$ is served as a likely threshold for achieving complete hydrogen coverage, and Fig. 7(f) illustrates the optimized configuration.

In general, the less charge injected into a conductor, the lower the amount of external energy required, and the lower the demands on the electronics, thus the easier it is to realize. Therefore, from a cost-effective point of view, the realization of adsorbing and releasing hydrogen during the conversion of neutral and $4e^-$ negatively charged C_9N_4 monolayers is a preferable option.

4 Conclusions

In summary, based on the DFT calculation results, we

demonstrate that modification in the charged condition enables C_9N_4 monolayer to achieve high-capacity hydrogen storage. This approach is experimentally feasible, possesses good reversibility, and exhibits fast kinetics. Specifically, the metallicity suggests that C_9N_4 possesses favorable electrical conductivity, enabling efficient electron injection and release for charge-controlled switchable hydrogen storage. During the H_2 adsorption process, introducing additional electrons into C_9N_4 causes the spontaneous binding of the H_2 molecule, exhibiting an exothermic nature. When extra electrons are extracted from negatively charged C_9N_4 monolayer, the H_2 molecule naturally revert to the state of weak bonding and detach from C_9N_4 monolayer. Moreover, the gravimetric density of stored hydrogen on $4e^-$ negatively charged C_9N_4 monolayer is up to 10.80 wt%, greatly surpassing the U.S. DOE standard and the values of many traditional hydrogen storage materials. Our work offers a potential solution to address the primary obstacles associated with mobile hydrogen storage.

Declarations The authors declare that they have no competing interests and there are no conflicts.

Electronic supplementary materials The online version contains supplementary material available at https://doi.org/10.1007/s11467-023-1385-0 and https://journal.hep.com.cn/fop/EN/10.1007/s11467-023-1385-0.

Acknowledgements We thank Jing Xue, Wanyi Zhao and Kaiyue Liu for their contributions to the image and text editions. The work was founded by Henan Scientific Research Fund for Returned Scholars, the Young Scientist Project of Henan Province (Grant No. 225200810103), the Program for Science & Technology Innovation Talents in Universities of Henan Province (Grant No. 24HASTIT013), Henan College Key Research Project (Grant No. 24A430002), the Natural Science Foundation of Henan Province (Grant No. 232300420128), the Scientific Research Innovation Team Project of Anyang Normal University (Grant No. 2023AYSYKYCXTD04), and the College Students Innovation Fund of Anyang Normal University (Grant No. 202310479077).

References

1. J. Tollefson, Hydrogen vehicles: Fuel of the future, *Nature* 464(7293), 1262 (2010)
2. L. Schlapbach and A. Züttel, Hydrogen-storage materials for mobile applications, *Nature* 414(6861), 353 (2001)
3. F. Schüth, B. Bogdanović, and M. Felderhoff, Light metal hydrides and complex hydrides for hydrogen storage, *Chem. Commun. (Camb.)* 2249(20), 2249 (2004)
4. F. Ding and B. I. Yakobson, Challenges in hydrogen adsorptions: From physisorption to chemisorption, *Front. Phys.* 6(2), 142 (2011)
5. X. Zhou, J. Zhou, and Q. Sun, Tripyrrylmethane based 2D porous structure for hydrogen storage, *Front. Phys.* 6(2), 220 (2011)
6. J. Li, T. Furuta, H. Goto, T. Ohashi, Y. Fujiwara, and S. Yip, Theoretical evaluation of hydrogen storage capacity in pure carbon nanostructures, *J. Chem. Phys.* 119(4), 2376 (2003)
7. P. Jena, Materials for hydrogen storage: Past, present, and future, *J. Phys. Chem. Lett.* 2(3), 206 (2011)
8. L. Wang and R. T. Yang, New sorbents for hydrogen storage by hydrogen spillover – a review, *Energy Environ. Sci.* 1(2), 268 (2008)
9. L. Song, C. Jiang, S. Liu, C. Jiao, X. Si, S. Wang, F. Li, J. Zhang, L. Sun, F. Xu, and F. Huang, Progress in improving thermodynamics and kinetics of new hydrogen storage materials, *Front. Phys.* 6(2), 151 (2011)
10. H. Zhang, X. Li, and Y. Tang, DFT study of dihydrogen interactions with lithium containing organic complexes $C_4H_{4-m}Li_m$ and $C_5H_{5-m}Li_m$ ($m = 1, 2$), *Front. Phys.* 6(2), 231 (2011)
11. M. Yoon, S. Yang, C. Hicke, E. Wang, D. Geohegan, and Z. Zhang, Calcium as the superior coating metal in functionalization of carbon fullerenes for high-capacity hydrogen storage, *Phys. Rev. Lett.* 100(20), 206806 (2008)
12. Q. Sun, P. Jena, Q. Wang, and M. Marquez, First-principles study of hydrogen storage on $Li_{12}C_{60}$, *J. Am. Chem. Soc.* 128(30), 9741 (2006)
13. Y. H. Cheng, C. Y. Zhang, J. Ren, and K. Y. Tong, Hydrogen storage in Li-doped fullerene-intercalated hexagonal boron nitrogen layers, *Front. Phys.* 11(5), 113101 (2016)
14. Z. Zhang, J. Li, and Q. Jiang, Density functional theory calculations of the metal-doped carbon nanostructures as hydrogen storage systems under electric fields: A review, *Front. Phys.* 6(2), 162 (2011)
15. Y. Zhao, Y. H. Kim, A. Dillon, M. Heben, and S. Zhang, Hydrogen storage in novel organometallic buckyballs, *Phys. Rev. Lett.* 94(15), 155504 (2005)
16. X. K. Kong, Q. W. Chen, and Z. Y. Lun, The influence of N-doped carbon materials on supported Pd: Enhanced hydrogen storage and oxygen reduction performance, *ChemPhysChem* 15(2), 344 (2014)
17. S. Li, H. Zhao, and P. Jena, Ti-doped nano-porous graphene: A material for hydrogen storage and sensor, *Front. Phys.* 6(2), 204 (2011)
18. Q. Sun, Q. Wang, P. Jena, and Y. Kawazoe, Clustering of Ti on a C_{60} surface and its effect on hydrogen storage, *J. Am. Chem. Soc.* 127(42), 14582 (2005)
19. Y. Zhang and H. Dai, Formation of metal nanowires on suspended single-walled carbon nanotubes, *Appl. Phys. Lett.* 77(19), 3015 (2000)
20. Q. Fu, L. Yuan, Y. Luo, and J. Yang, Exploring at nanoscale from first principles, *Front. Phys. China* 4(3), 256 (2009)
21. M. Yoon, S. Yang, E. Wang, and Z. Zhang, Charged fullerenes as high-capacity hydrogen storage media, *Proc. Natl. Acad. Sci. USA* 7(9), 2578 (2007)
22. J. Niu, B. Rao, and P. Jena, Binding of hydrogen molecules by a transition-metal ion, *Phys. Rev. Lett.* 68(15), 2277 (1992)
23. J. Zhou, Q. Wang, Q. Sun, P. Jena, and X. Chen, Electric field enhanced hydrogen storage on polarizable materials

substrates, *Proc. Natl. Acad. Sci. USA* 107(7), 2801 (2010)
24. H. Cheng and J. C. Zheng, *Ab initio* study of anisotropic mechanical and electronic properties of strained carbon–nitride nanosheet with interlayer bonding, *Front. Phys.* 16(4), 43505 (2021)
25. Z. Ma, J. Zhuang, X. Zhang, and Z. Zhou, SiP monolayers: New 2D structures of group IV–V compounds for visible-light photohydrolytic catalysts, *Front. Phys.* 13(3), 138104 (2018)
26. Q. Gao, H. L. Wang, L. F. Zhang, S. L. Hu, and Z. P. Hu, Computational study on the half-metallicity in transition metal–oxide-incorporated 2D g-C_3N_4 nanosheets, *Front. Phys.* 13(3), 138108 (2018)
27. L. Ju, C. Liu, L. Shi, and L. Sun, The high-speed channel made of metal for interfacial charge transfer in Z-scheme g-C_3N_4/MoS_2 water-splitting photocatalyst, *Mater. Res. Express* 6(11), 115545 (2019)
28. C. He, J. H. Zhang, W. X. Zhang, and T. T. Li, Type-II InSe/g-C_3N_4 heterostructure as a high-efficiency oxygen evolution reaction catalyst for photoelectrochemical water splitting, *J. Phys. Chem. Lett.* 10(11), 3122 (2019)
29. J. Liu, B. Cheng, and J. Yu, A new understanding of the photocatalytic mechanism of the direct Z-scheme g-C_3N_4/TiO_2 heterostructure, *Phys. Chem. Chem. Phys.* 18(45), 31175 (2016)
30. G. Zhang, M. Zhang, X. Ye, X. Qiu, S. Lin, and X. Wang, Iodine modified carbon nitride semiconductors as visible light photocatalysts for hydrogen evolution, *Adv. Mater.* 26(5), 805 (2014)
31. J. Sun, J. Zhang, M. Zhang, M. Antonietti, X. Fu, and X. Wang, Bioinspired hollow semiconductor nanospheres as photosynthetic nanoparticles, *Nat. Commun.* 3(1), 1139 (2012)
32. X. Ye, Y. Cui, and X. Wang, Ferrocene-modified carbon nitride for direct oxidation of benzene to phenol with visible light, *ChemSusChem* 7(3), 738 (2014)
33. J. Zhang, Y. Chen, and X. Wang, Two-dimensional covalent carbon nitride nanosheets: Synthesis, functionalization, and applications, *Energy Environ. Sci.* 8(11), 3092 (2015)
34. S. P. Kaur, T. Hussain, T. Kaewmaraya, and T. J. D. Kumar, Reversible hydrogen storage tendency of light-metal (Li/Na/K) decorated carbon nitride (C_9N_4) monolayer, *Int. J. Hydrogen Energy* 48(67), 26301 (2023)
35. J. Huang, C. Zhou, and X. Duan, Li decorated C_9N_4 monolayer as a potential material for hydrogen storage, *Int. J. Hydrogen Energy* 46(65), 32929 (2021)
36. X. Tan, L. Kou, H. A. Tahini, and S. C. Smith, Charge modulation in graphitic carbon nitride as a switchable approach to high-capacity hydrogen storage, *ChemSusChem* 8(21), 3626 (2015)
37. P. E. Blöchl, Projector augmented-wave method, *Phys. Rev. B* 50(24), 17953 (1994)
38. J. P. Perdew and Y. Wang, Accurate and simple analytic representation of the electron-gas correlation energy, *Phys. Rev. B* 45(23), 13244 (1992)
39. J. Heyd, G. E. Scuseria, and M. Ernzerhof, Hybrid functionals based on a screened Coulomb potential, *J. Chem. Phys.* 118(18), 8207 (2003)
40. S. Grimme, Semiempirical GGA-type density functional constructed with a long-range dispersion correction, *J. Comput. Chem.* 27(15), 1787 (2006)
41. S. Liu, H. Yin, and P. F. Liu, Strain-dependent electronic and mechanical properties in one-dimensional topological insulator Nb_4SiTe_4, *Phys. Rev. B* 108(4), 045411 (2023)
42. L. Ju, Y. Ma, X. Tan, and L. Kou, Controllable electrocatalytic to photocatalytic conversion in ferroelectric heterostructures, *J. Am. Chem. Soc.* 145(48), 26393 (2023)
43. B. Mortazavi, M. Shahrokhi, A. V. Shapeev, T. Rabczuk, and X. Zhuang, Prediction of C_7N_6 and C_9N_4: Stable and strong porous carbon-nitride nanosheets with attractive electronic and optical properties, *J. Mater. Chem. C* 7(35), 10908 (2019)
44. M. Yoon, S. Yang, E. Wang, and Z. Zhang, Charged fullerenes as high-capacity hydrogen storage media, *Nano Lett.* 7(9), 2578 (2007)
45. Y. Liu, L. Ren, Y. He, and H. P. Cheng, Titanium-decorated graphene for high-capacity hydrogen storage studied by density functional simulations, *J. Phys.: Condens. Matter* 22(44), 445301 (2010)
46. L. Bi, Z. Miao, Y. Ge, Z. Liu, Y. Xu, J. Yin, X. Huang, Y. Wang, and Z. Yang, Density functional theory study on hydrogen storage capacity of metal-embedded penta-octa-graphene, *Int. J. Hydrogen Energy* 47(76), 32552 (2022)
47. N. Khossossi, Y. Benhouria, S. R. Naqvi, P. K. Panda, I. Essaoudi, A. Ainane, and R. Ahuja, Hydrogen storage characteristics of Li and Na decorated 2D boron phosphide, *Sustain. Energy Fuels* 4(9), 4538 (2020)
48. S. Haldar, S. Mukherjee, and C. V. Singh, Hydrogen storage in Li, Na and Ca decorated and defective borophene: A first principles study, *RSC Adv.* 8(37), 20748 (2018)